iScience

CellPress
OPEN ACCESS

Article

Revealing *in vivo* cellular mechanisms of cerebral microbleeds on neurons and microglia across cortical layers

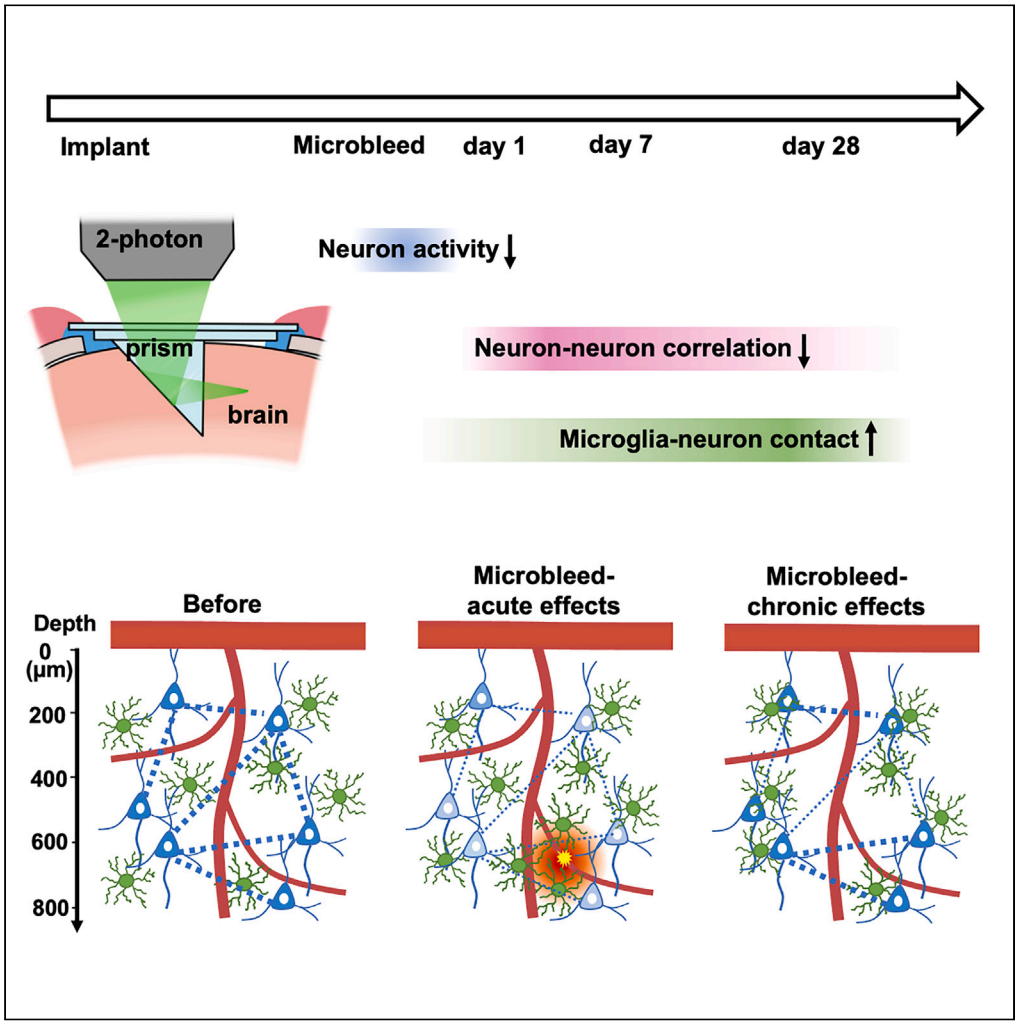

Qianru Yang, Alberto L. Vazquez, X. Tracy Cui

alv15@pitt.edu (A.L.V.)
xic11@pitt.edu (X.T.C.)

Highlights

Two-photon microscopy and microprism unveil deep cortical CMB effects in awake mice

CMBs suppress neuronal activity and impact neuron-neuron correlations

Microglial contact with neurons increases, while surveillance is unchanged by CMBs

CMB disrupts the negative correlation between neuron firing and microglial contact

Yang et al., iScience *27*, 109371
April 19, 2024
https://doi.org/10.1016/j.isci.2024.109371

iScience

CellPress
OPEN ACCESS

Article

Revealing *in vivo* cellular mechanisms of cerebral microbleeds on neurons and microglia across cortical layers

Qianru Yang,[1,2,3] Alberto L. Vazquez,[3,4,5,*] and X. Tracy Cui[2,3,5,6,*]

SUMMARY

Cerebral microbleeds (CMBs) are associated with higher risk for various neurological diseases including stroke, dementia, and Alzheimer's disease. However, the understanding of cellular pathology of CMBs, particularly in deep brain regions, remains limited. Utilizing two-photon microscopy and microprism implantation, we longitudinally imaged the impact of CMBs on neuronal and microglial activities across cortical depths in awake mice. A temporary decline in spontaneous neuronal activity occurred throughout cortical layers, followed by recovery within a week. However, significant changes of neuron-neuron activity correlations persisted for weeks. Moreover, microglial contact with neuron soma significantly increased post-microbleeds, indicating an important modulatory role of microglia. Notably, microglial contact, negatively correlated with neuronal firing rate in normal conditions, became uncorrelated after microbleeds, suggesting a decreased neuron-microglia inhibition. These findings reveal chronic alterations in cortical neuronal networks and microglial-neuronal interactions across cortical depths, shedding light on the pathology of CMBs.

INTRODUCTION

Cerebral microbleeds (CMBs) are focal ruptures of small vessels in the brain. They have been identified as significant indicators of aging,[1] cognitive dysfunction,[2,3] and various neurovascular and neurodegenerative diseases.[4–8] For instance, CMBs are present in 5% of healthy adults, 29% of individuals with Alzheimer's disease, 52% of patients experiencing a first-ever intracerebral hemorrhage (ICH), and 83% of those with recurrent ICH.[9,10] In the field of neural engineering, the implantation of penetrating neural electrodes for brain–computer interfaces inevitably leads to blood vessel disruption,[11] while the presence of stiff implants can lead to spontaneous capillary damage or persistent blood-brain barrier (BBB) leakage. Higher levels of BBB damage have been associated with more pronounced inflammatory responses and compromised performance of neural interfaces.[11–13] BBB disruption not only impairs normal substrate circulation but also triggers the release of neurotoxic blood-derived products, cells, and pathogens into the brain, initiating inflammatory responses and neurodegenerative pathways.[14,15] Understanding the intricate relationship between the vascular system and brain health is crucial for unraveling the mechanisms underlying these pathologies and developing effective therapeutic strategies.

Microglia, the resident immune cells in the brain parenchyma, play essential roles in maintaining brain homeostasis. They engage in bidirectional communication with neurons through various immunomodulatory factors and signaling pathways, influencing both normal physiology and pathological conditions.[16–18] During brain development, microglia are involved in the pruning of excessive synapses.[19,20] In the healthy brain, microglia dynamically survey their surroundings through ramified processes.[21,22] Microglia can suppress excessive neuronal activity by sensing and catabolizing extracellular ATP.[23] Also, healthy neurons can inhibit microglial immune activation via direct cell-cell contact or ligand-receptor interaction.[24,25] Neuronal activity can steer microglial processes toward the highly active neuron soma, which in turn downregulates the activity of contacted neurons.[26] Under pathological conditions such as ischemic stroke, the disappearance of neuronal inhibition signals leads to microglial activation.[24,25] Damaged neurons can also produce signals to activate microglial functions.[27] Activated microglia undergo morphological changes, including extending processes, migration toward the injury, and transformation into enlarged cell bodies with retracted processes for phagocytosis.[28–31] The role of activated microglia is 2-fold, as they can release proinflammatory cytokines and cytotoxic substances detrimental to neuronal survival,[32–35] while also promoting tissue repair through phagocytosis and production of anti-inflammatory factors and growth factors.[36–38] The absence of microglia in a mouse stroke model resulted in increased infarct size and neuronal death, highlighting their protective role after brain injury.[36] Microglial activation preconditioning has shown to protect the brain

[1]Department of Neurosurgery, Stanford University, Palo Alto, CA, USA
[2]Department of Bioengineering, University of Pittsburgh, Pittsburgh, PA, USA
[3]Center for Neural Basis of Cognition, University of Pittsburgh and Carnegie Mellon University, Pittsburgh, PA, USA
[4]Department of Radiology, University of Pittsburgh, Pittsburgh, PA, USA
[5]McGowan Institute for Regenerative Medicine, University of Pittsburgh, Pittsburgh, PA, USA
[6]Lead contact
*Correspondence: alv15@pitt.edu (A.L.V.), xic11@pitt.edu (X.T.C.)
https://doi.org/10.1016/j.isci.2024.109371

from subsequent injuries.[39,40] The concept of microglial differential polarization suggests that microglia can shift between pro-inflammatory and anti-inflammatory phenotypes, depending on the nature and duration of the stimulus.[41,42] However, more *in vivo* research is needed to fully elucidate the process and mechanisms underlying microglial phenotype transformations.[42,43]

In vivo two-photon microscopy (TPM) has emerged as a valuable tool for observing cellular activities in live animals.[44,45] Additionally, the use of ultra-short high-power laser pulses allows for controlled ablation of single microvessels in the brain, providing a reliable model for studying microbleeds.[46–48] Previous studies have focused on understanding the responses of neurons and glial cells in the superficial cortex (L2/3) to microbleeds. These studies have shown that in the vicinity of microbleeds, there is a temporary loss of astrocytes and a decrease in evoked neuron calcium responses, which quickly recovers within one day.[49] However, no degenerative morphological changes were observed in neural dendrites near the micro hemorrhage.[50] Microglia, on the other hand, respond quickly to microbleeds by extending processes, followed by migration and proliferation over hours to days.[30] However, the tissue responses to microbleeds in the deep cortex remain largely unknown.[51] Due to light scattering and absorption in the tissue, high-quality TPM is typically limited to superficial layers (up to layer 2/3 of the cortex) in chronic setups. It is important to note that the responses observed in superficial layers may not necessarily be the same as those in deep layers. The neocortex consists of six laminar layers, each with diverse compositions of neuron subtypes and distinct anatomical structures that contribute to diverse roles in cortical neuronal network computations.[52–54] Simultaneous monitoring of neuronal activity across all the cortical layers is essential for a comprehensive understanding of the cortical network.[55–57] In addition, cortical neurons in different layers possess diverse connections to other brain regions. Layer 2/3 pyramidal neurons extensively project parallel axons to other cortical regions, while layer 5/6 pyramidal neurons extend axonal projections to not only other cortical regions, but subcortical regions including striatum and thalamus.[58] The presence of microbleeds in deep cortical layers may have consequences influencing the functional integrity of these distant brain areas. The cortical vasculature is also depth dependent, with main arteries and veins located on the brain's surface penetrating down into the deep cortex for blood circulation. The blood flow speed and the topological structure of blood vessels differ significantly between superficial layers and deep layers of the cortex.[59,60] As a result, the pathological tissue responses to microbleedings in superficial layers and deep layers could be substantially different.

This work aims to investigate the influence of deep cortical microbleeds on the function of neurons and microglia across all cortical depths. To achieve this, we employed a microprism implantation to visualize cellular activities across all cortical layers simultaneously. Microprism is an optical device that turns the optical path by 90°, allowing in-plane imaging along depth.[29,61,62] A 1 mm microprism can technically reach 1 mm deep into the brain, covering all cortical depths and potentially some white matter regions in mice. Previous research has shown that the inflammatory responses associated with chronic microprism implantations resolve within several weeks using intravital TPM imaging in mice.[29] In the current study, we investigated the consequences of deep cortical microbleedings on both neuronal and microglial activities across all cortical depths in live mice for a period of up to 4 weeks. We found an initial decline in the spontaneous neuronal activity and a reduction in neuronal firing rates, followed by a subsequent recovery within a week. However, there was a persistent and significant decrease in the activity correlation between neuron pairs within the same layer and across different layers following microvessel injury. This finding suggests that microbleeds in the deep cortex can disrupt the functional connectivity of neurons throughout all cortical depths, impairing the coordinated activity of neuronal networks. Additionally, microglial contact with neuronal soma increased substantially after one week, while the overall surveillance level of microglia remained unchanged, suggesting that microglia specifically target and interact with neuronal soma in response to microbleeds. Prior to the injury, there was a negative correlation between microglial contact and neuronal firing rate, but this relationship underwent significant changes shortly after the onset of microbleeds. This indicates that microbleeds alter microglia-neuron interactions, which can impact neuronal function. Overall, this work significantly enhances our understanding of the chronic influence of deep cortical microvessel injury on neuronal networks and the interaction between neurons and microglia across cortical depths.

RESULTS

Experiment setup

To image both microglia and neurons simultaneously, we crossed CX3CR1-GFP mice with Thy1-jRGECO1a mice. We performed microprism implantation surgery on three adult mice (8–20 weeks) and let them recover for ~5–8 weeks before we generated a microbleed in the deep cortex by laser ablation of the vessel wall. During the recovery period, the animal was habituated to weekly head-fixed for two-photon imaging on a treadmill. Two-photon imaging in awake animals was conducted at multiple time points before and after laser ablation as shown in Figure 1A. The surgical procedure for microprism implantation has been previously described in several publications.[29,61,62] In our study, a 3 by 3 mm craniotomy was performed, followed by the implantation of a 1 mm microprism oriented toward the visual cortex. The microprism turns the light path by 90° to present a vertical plane that allows imaging of all cortical layers at the same time. The cranial window was sealed with Kwik-Sil and dental cement for longitudinal imaging (Figure 1B). In accordance with previous studies using microprism implantation, we have a clear, stable imaging window for many weeks. After the recovery period, the distribution of microglia and firing neurons exhibited minimal disparities when assessed one week apart (Figure 1C).

Deep CMBs result in an acute decrease in spontaneous neuronal activity

To visualize blood vessels in the brain, we injected Cascade Blue dextran dye intraperitoneally (IP) (Figure 2A). Focal microbleeds in layer 5/6 were induced by focusing the two-photon laser over a single point on the wall of small blood vessels (d = 14.87 ± 5.20 μm, Figure 2B) following previously well-established protocols.[29,46] The power and duration were gradually increased until a sudden increase in fluorescence intensity occurred, indicating leakage of the vascular dye. These microbleeds in the deep cortex (depth = 688 ± 21 μm, Figure 2C) often show a dark surrounding acutely (Figure 2D), presumably due to the leakage of light-absorbing red blood cells.

CellPress
OPEN ACCESS

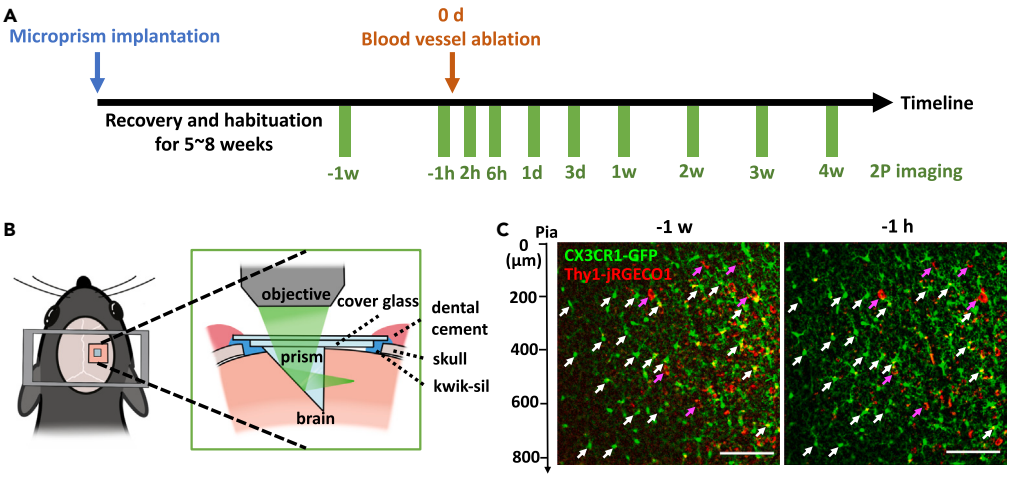

Figure 1. Microprism implantation enables imaging of neurons and microglia throughout cortical layers

(A) Timeline of experiments.

(B) Schematic of microprism implantation and two-photon imaging in head-fixed, awake mice.

(C) Representative two-photon image of neurons and microglia in transgenic mice expressing CX3CR1-GFP and Thy1-jRGECO1a before laser ablation 100 μm away from the microprism. Note the similar distribution of active neurons (magenta arrows) and microglia (white arrows) with one week apart. Scale bar = 200 μm. Abbreviations: h hour, d day, w week, 2P two-photon.

We first examined how these microbleeds in deep cortex affect neural activity over time. TPM images were acquired about 100 μm away from the microprism. According to our previous study, microglia located 100 μm away from the microprism took approximately 6 weeks to recover and return to their homeostatic state.[29] Active neurons were identified manually from a 20-min TPM imaging session at a single plane of spontaneous neural calcium activity at each time point. The same field of view (FOV) was tracked over time using a combination of references, including the distance from the microprism surface, vascular landmarks, microglial distribution and the location of the ablation point (Figure 2D). We quantified the number of active neurons in three animals, starting one week before the laser induced CMBs and continuing for a duration of four weeks. In one of the animals, the two-photon imaging data was lost at week 2 due to technical issues. As a result, we excluded the week 2 data from the quantitative analysis. The total number of active neurons in our 815 × 815 μm FOV decreased significantly at 2 h and 6 h compared to 1h prior to CMBs (Figure 2E). Within 150 μm from the microbleed, the average number of spontaneously active neurons dropped from 4 to 6 neurons before the damage, to 0–1 neuron between 2 h and 3 days (with 6 h and 1 day showing statistical significance compared to -1h) and began to show a trend of recovery from 1 w to 4 w (Figure 2F).

To examine any potential changes in the layer distribution of active neurons within the cortical column of the microbleed over time, we generated a plot depicting the depth of individual neurons within a 400 μm wide column centered at the microbleed (Figure 2G). Following the injury, we observed a decrease in the number of active neurons across all the depths from 2 h to 1 day post-injury. Here, depth was normalized to the depth of the injury (0 μm).

Furthermore, to examine whether the firing rates of these neurons alter over time, we quantified the cumulative calcium fluorescence intensity changes (cumulative ΔF/F) above the threshold (mean +SD) of spontaneously active neurons (Figures 3A and 3B). According to the previous literature, the ΔF/F peak amplitude is roughly proportional to the number of spikes.[63] Therefore, the cumulative ΔF/F indicates the total number of spikes during the imaging session for each neuron. The cumulative ΔF/F was significantly reduced at 6 h post blood vessel damage and then back to normal after 1 day (Figure 3C), indicating a transient decrease of neural firing rate at around 6 h post injury. These results show that deep cortical microbleeds have the potential to cause acute impairment in both the number and the firing rate of spontaneously active neurons surrounding the injury.

Deep CMBs induce prolonged alterations in neuron-neuron activity correlations post-recovery of neuronal spontaneous activity

To investigate the functional changes in cortical neural circuits, we conducted an analysis of calcium activity correlations among paired neurons within the same layer and across different layers. To ensure an adequate number of neurons for analysis, we categorized neuron depth into three major layers: superficial layer (S; >400 μm), middle layer (M; >200 μm and <400 μm), and deep layer (D; <200 μm) according to the depth of the neuron relative to the CMB (Figure 4A).

During the pre-injury period, the six types of paired correlation (SS, MM, DD, SM, SD, and MD) exhibited similar patterns and showed minimal changes over time. However, at three days post-injury, several types of neuron correlations demonstrated a significant decrease compared to 1 h before the injury (Figure 4B). Subsequently, at 3 w and 4 w post-injury, there was a recovery in activity correlation among most depth pairs, except for the SM correlation at 3 w and the SD correlation at 4 w. Notably, we observed a hyper correlation in MM at both 3 w and 4 w.

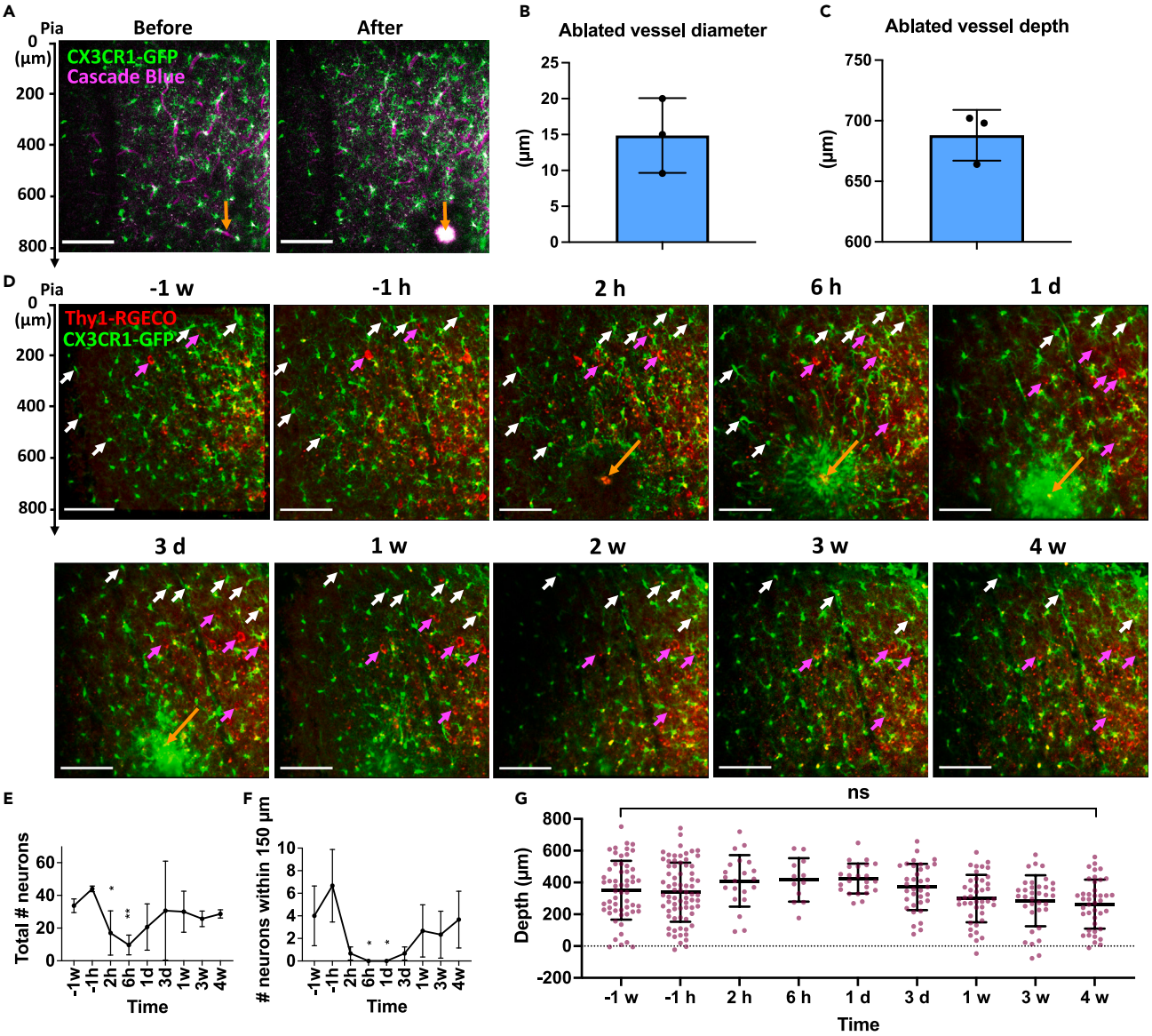

Figure 2. The number of spontaneously active neurons decreased acutely after deep CMBs

(A) Immediately before and after generation of a microbleed by point-laser ablation. Arrows indicate the laser ablation site. Scale bar = 200 µm. Green: microglia labeled by CX3CR1-GFP. Magenta: blood vessels labeled by Cascade Blue-dextran dye.

(B) Quantification of ablated blood vessel diameters. d = 14.87 ± 5.20 µm. Data are presented as mean ± standard deviation (STD). N = 3 animals.

(C) The depth of ablation points from the pia. Depth = 688 ± 21 µm. Data are presented as mean ± STD. N = 3 animals.

(D) Representative TPM images of microglia (green) and spontaneous neural calcium activities (red) max-projected from 20-min long scans. The same field of view were tracked over time by monitoring the distance from the microprism, microglial distribution (representative white arrows) and the ablated point (orange arrows). Magenta arrows highlight several representative neurons that are potentially the same cell across multiple time points. Scale bar = 200 µm.

(E) Total number of active neurons in our FOV over time. Data are presented as mean ± STD. N = 3 animals. One-way ANOVA ($p = 0.0245$) followed by Dunn's multiple comparison test comparing each time point to −1 h. $p = 0.023$ (*) at 2 h and $p = 0.0083$ (**) at 6 h.

(F) Number of active neurons within 150 µm radius from the microbleed. Data are presented as mean ± STD. N = 3 animals. One-way ANOVA ($p = 0.0133$) followed by Dunn's multiple comparison test comparing each time point to −1 h. $p = 0.0179$ (*) at 6 h and $p = 0.0179$ (**) at 1 day.

(G) Distribution of spontaneously active neurons along depth over time. Data are presented as mean ± STD. N = 29 to 132 neurons from 3 animals. One-way ANOVA ($p = 0.0056$) followed by Dunn's multiple comparison test comparing each time point to −1 h.

To explore whether the changes in depth correlations were associated with alterations in neuron firing rates across different layers, we also quantified the cumulative ΔF/F for each major layer over time (Figure 4C). The results indicated that, for the most part, the average neuron firing rates remained similar to those observed before the injury. The only significant change was an increase in neuron firing rate in the

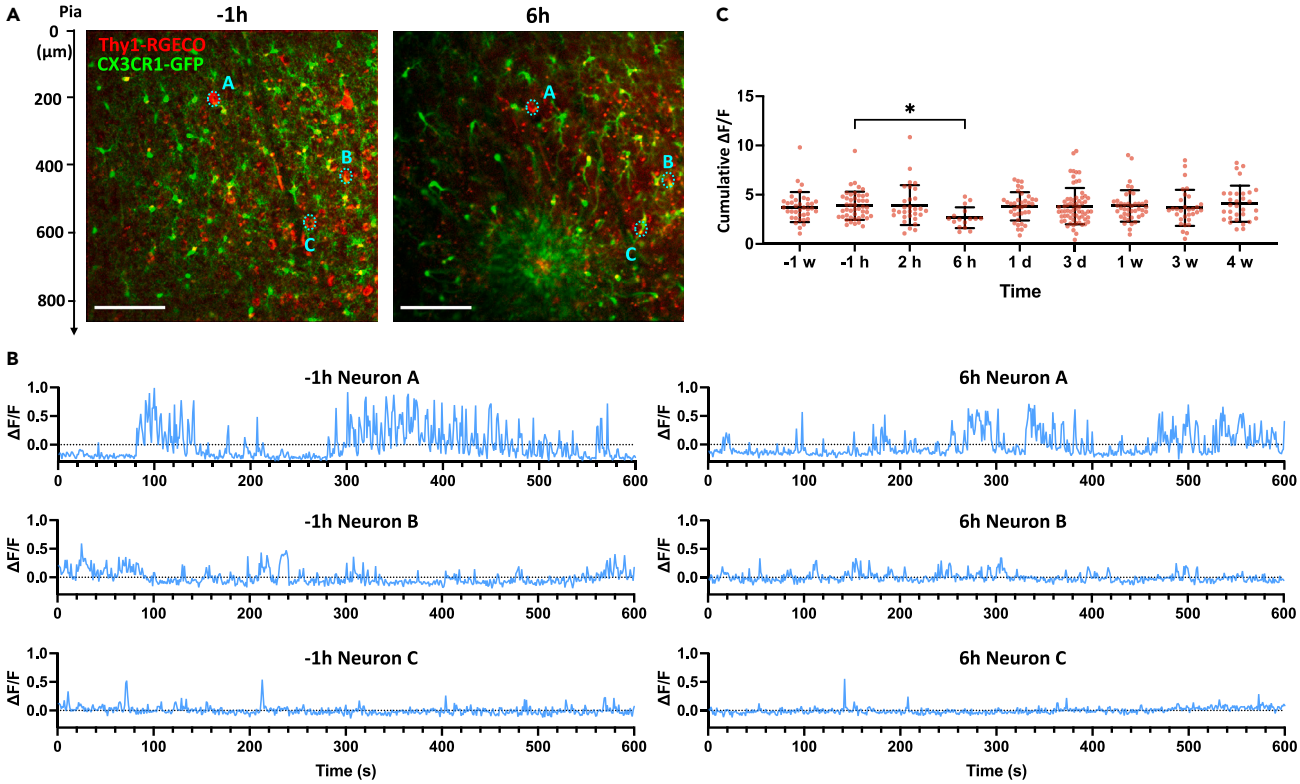

Figure 3. The firing rate of spontaneous neural activities decreased acutely after deep CMBs

(A) TPM images of microglia (green) and spontaneous neural calcium activities (red) max-projected from 20-min long scans at -1h and 6h after microbleeds. Three representative neurons (dotted cyan circles) were identified. Scale bar = 200 μm.

(B) Normalized neuronal calcium fluorescence activity of the three representative neurons at -1h and 6h.

(C) Neuronal firing rate indicated by accumulative ΔF/F over time. Data are presented as mean ± STD. N = 29 to 132 neurons from 3 animals. One-way ANOVA ($p = 0.1743$) followed by Dunn's multiple comparison test comparing each time point to −1 h. $p = 0.0231$ (*) at 6 h. The p value was adjusted to account for multiple comparisons.

superficial layer at week 4, which is unlikely to be the cause for the decrease in SD correlation. These results suggest that the correlation levels of neuron activity significantly decreased in almost all types of intra-layer and inter-layer neuron pairs after deep CMBs, without affecting the neuronal firing rates. These decreases in correlations partially recovered over the more chronic phase, but inter-layer correlations (SM and SD) remained dampened at week 3 and week 4, respectively.

Spatial distribution of microglia and neurons changes after CMBs

Microglia, the resident inflammatory cells in the brain, play important roles in regulating tissue immune responses after injury. We observed microglia respond first by sending processes toward the damaged blood vessel. Within several hours, they migrated and formed a dense encapsulation around the CMB by 6 h (Figure 5A). The microglial migration dynamics and time course have been characterized in detail in our previous study using a similar setup.[29] Here, we focus on the microglia-neuron interactions. We first noticed that the spatial distribution of microglia and neurons changes after CMBs. Before laser ablation, microglia and active neurons scattered nearly evenly accross all depths (Figure 5B). 2 h post CMB, the number of active neurons decreased in both deep layers and superficial layers. Meanwhile, the microglial intensity distribution did not change much (Figure 5B). After 6 h, neurons across all layers were more silent and microglia gathered around the CMB. From day 1 to day 7 (1 w), microglial intensity remained high near the CMB, and neuronal activity started to recover, most evidently in the middle layers. After about 3 weeks, microglial encapsulation went down, but the active neurons were still concentrated in the middle layers. The sustained changes of the spatial distribution of active neurons along depth suggest that CMBs at the deep cortical layer could introduce long-term alterations in the cortical network activity.

Neuron-microglia dynamic interaction changes after CMBs

Next, we aimed to investigate the changes in the interaction between neurons and microglia following deep cortical microbleeds. In their homeostatic state, microglia establish frequent contact with synapses and participate in the assay and elimination of synapses.[40,64] Microglia also interact with neuronal somata in healthy conditions, with processes making contact with neuronal somatic cell membrane that can rapidly undergo

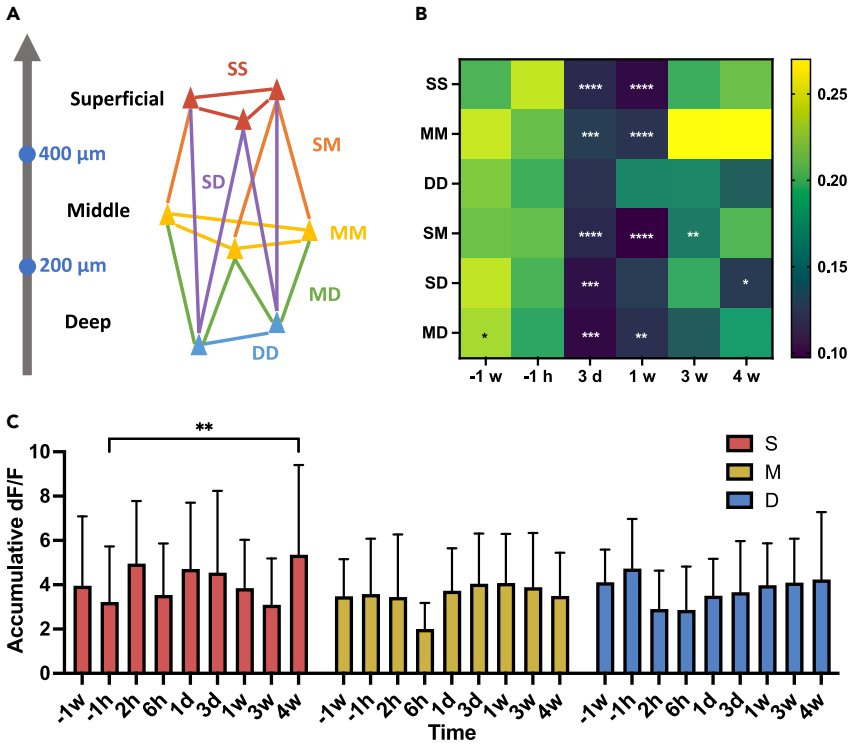

Figure 4. Activity correlation of cortical neural circuit changes after CMBs

(A) Schematic showing the category of neuronal correlation.

(B) The average absolute value of the correlation coefficient of the six types of neuronal activity correlation over time. N = 4–264 neuron pairs (mean = 73) from 3 animals. One-way ANOVA followed by multiple comparison test, comparing every time point to −1 h within the same correlation type. *p < 0.05, **p < 0.01, ***p < 0.001, ****p < 0.0001. Each p value was adjusted to account for multiple comparisons.

(C) The average cumulative ΔF/F in the three major layers, superficial (S), middle (M), and deep (D) over time. Two-way ANOVA followed by Sidak's multiple comparisons test, comparing every time point to −1 h within each layer. **p = 0.0088.

alterations in response to brain injury.[65] To quantify the extent of microglia-neuron soma contact, we assessed the microglial contact area ratio within each neuronal soma over a 20-min TPM imaging session at each time point (Figure 6A). Before CMBs, the microglial contact ratio with the soma of active neurons is close to 0 (Figure 6B). After CMBs are introduced, microglial contact with neurons significantly increased at 6 h and from 1 w to 4 w (Figure 6B). When examining the depth distribution of the microglia-neuron soma contact ratio over time, we observed that these increases were consistent across different depths (Figure 6C). We then tested whether this overall contact elevation between microglia and active neuron soma resulted from a general increase in microglial surveillance. To quantify the microglial surveillance level, we took standard deviation

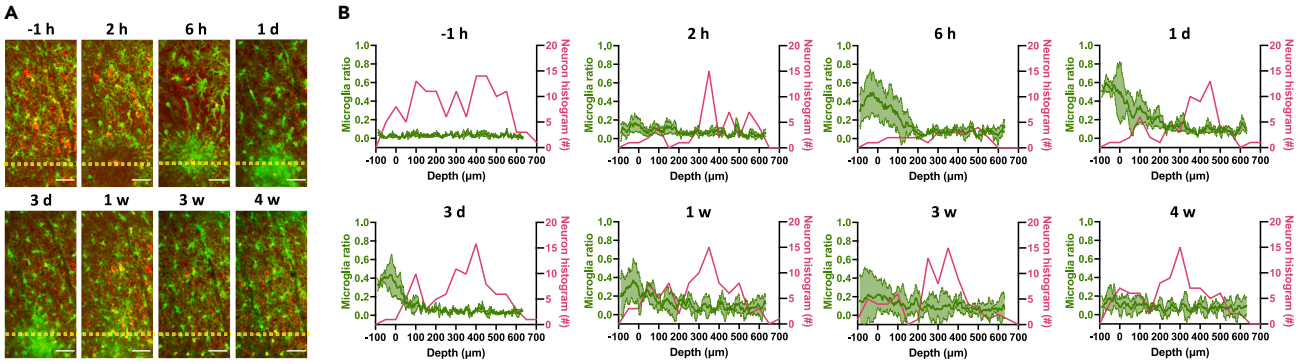

Figure 5. The distribution of microglia and active neurons along depth changes over time

(A) Representative images of microglia superimposed with spontaneously active neurons. Green: CX3CR1-GFP. Red: Thy1-jRGECO1a. Yellow lines indicate the depth of the microbleed. Scale bar = 100 µm.

(B) Distribution of microglial fluorescence ratio (green) and the average number of active neurons (pink) along the depth. The depths were normalized to the location of blood vessel damage across different animals. Microglial fluorescence ratio are presented as mean ± STD. N = 3 animals.

CellPress
OPEN ACCESS

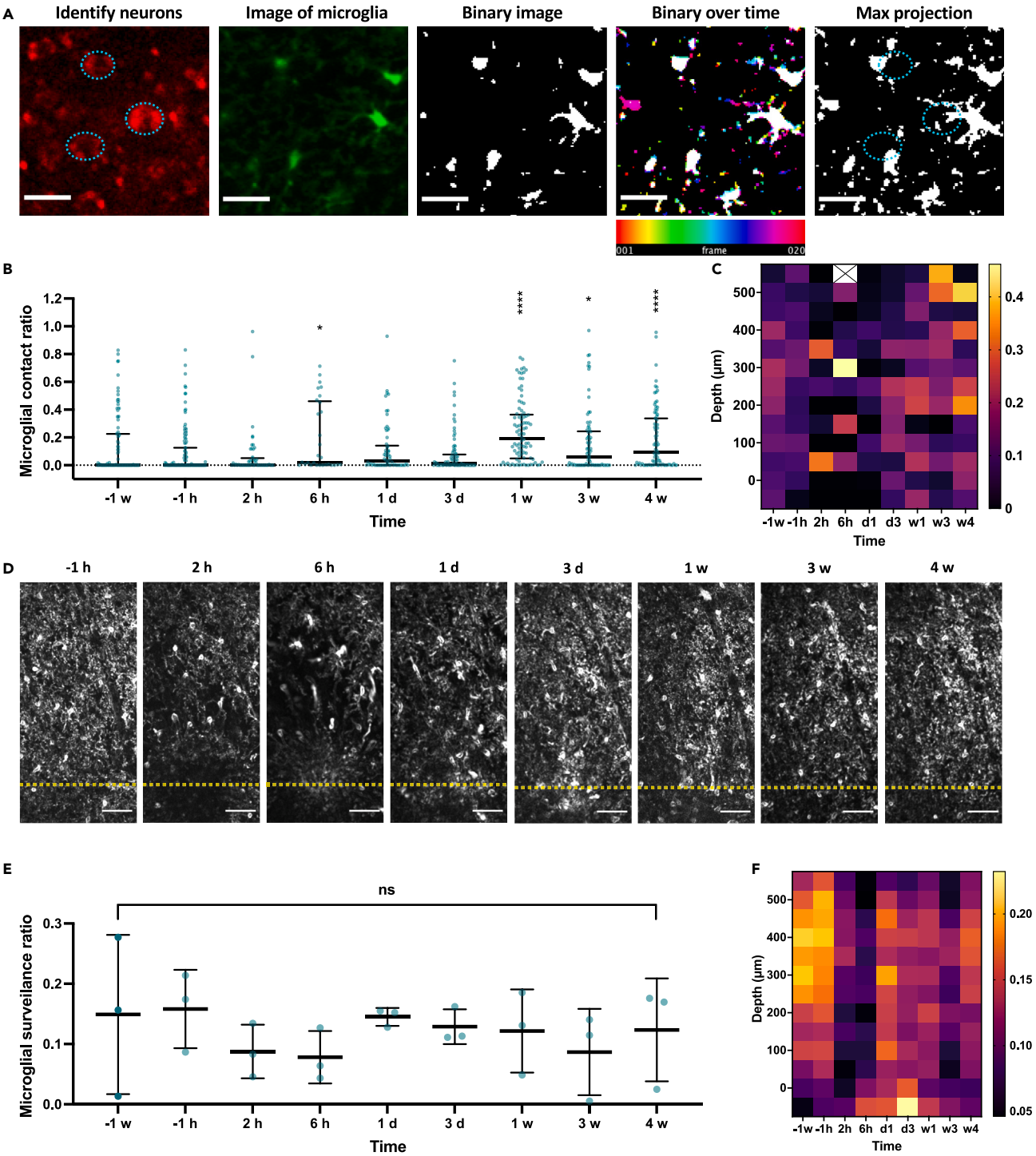

Figure 6. Increased microglial contact with neuron soma but not microglial surveillance after microbleeds

(A) Steps to calculate the microglial contact ratio on neuron soma. Neuron somata (cyan circles) are identified manually over the 20-min time-lapse video. Microglia images are binarized at each minute and max-projected to a single image. The microglia-neuron contact ratio is calculated by dividing the microglia area within each neuron soma from the microglial max projection over the total area of the neuron soma. Scale bar = 50 μm.

(B) The microglial contact ratio on neural soma over time. Data are presented as mean ± STD. N = 29–132 neurons from 3 animals. One-way ANOVA ($p < 0.0001$) followed by Dunn's multiple comparison test comparing each time point to −1 h. $p = 0.0256$ (*) at 6 h, $p < 0.0001$ (****) at 1 w and 4 w, and $p = 0.0159$ (*) at 3 w. Each p value was adjusted to account for multiple comparisons.

(C) The heatmap of microglial contact ratio on neural soma along depth over time. The mean value was calculated from 3 animals.

Figure 6. *Continued*

(D) Standard deviation projections of microglial fluorescence from a 20 min two-photon imaging over time. Yellow dotted lines indicate the depth of the microbleed. Scale bar = 100 μm.

(E) Microglial surveillance ratio calculated from the standard deviation projection images over the ~300 μm wide cortical column. Data are presented as mean ± STD. N = 3 animals. One-way ANOVA ($p = 0.6224$) followed by Dunn's multiple comparison test comparing each time point to −1 h.

(F) The heatmap of microglial surveillance ratio along depth over time. Averaged from 3 animals.

projections of microglia fluorescence from the 20-min TPM videos (Figure 6D). After applying a threshold, we calculated the average microglial surveillance ratio across the entire cortical column (Figure 6E) and binned the data based on different depths (Figure 6F). Before microbleeds, the microglial surveillance ratio showed higher values in the superficial cortex than the deeper layers, indicating that microglial dynamics could differ across cortical depths. Surprisingly, the microglial surveillance level did not exhibit an increase but rather a decrease trend, with no significant differences detected after microbleed onset. Furthermore, the heatmap of the microglial surveillance ratio distribution along depth over time differed significantly from the heatmap of microglia contact ratio. These results suggest that microglia specifically increase contact with neuron soma after CMBs.

In order to explore the potential relationship between microglial contact and neuronal activity, we examined the correlation between microglial contact area ratio and the cumulative ΔF/F (firing rate) for all the individual neurons over time (Figures 7A–7I). Prior to the blood vessel ablation (−1 w and −1 h), there was a significant negative correlation between microglial contact and neuronal activity ($p < 0.05$) (Figures 7A and 7B). This negative correlation agrees with previous literature where microglia can suppress neuronal activity.[23,26] After the occurrence of CMBs, the negative correlation remained significant at 2 h post-injury but was not significant from 6 h to 4 w post-injury (Figures 7C–7I). The Spearman correlation (r) between microglial contact and neuronal firing rate exhibited a steep change from approximately −0.3 to near zero between 2 h and 6 h post-injury, and the p value increased from below 0.05 to around 1, indicating a drastic change in the inhibitory microglia-neuron interaction during this early period. From 6 h to 1 w, the Spearman correlation coefficient remained close to zero and the p value stayed above 0.4, suggesting that the altered interaction between microglia and neuronal firing rate could persist for a certain duration. After 1 week, the Spearman correlation gradually decreased, and the p value continuously decreased as well, indicating a recovery trend. By 4 weeks post-injury, the correlation coefficient and p value were close to the levels observed before injury. Additionally, the microglial contact was not significantly correlated with the depth at any time points (Figure S1).

DISCUSSION

In this study, we investigated the impact of deep CMBs on the *in vivo* activity of neurons and microglia across cortical depth. To achieve this, we employed microprism implantation, which enabled simultaneous visualization of cellular activities from the brain surface to a depth of approximately 800 μm. This innovative approach not only allowed us to access deeper tissue with high SNR and relatively low power than conventional TPM, but also facilitated the study of intricate multi-layer cellular network interactions. Our investigation yielded several noteworthy findings.

First, we observed a temporary loss in the population of spontaneously active neurons and a decrease in their firing rate in the first several days following the micro vessel injury. This decline in neuronal calcium activity was not localized but occurred universally across all cortical layers. In the semi-chronic phase (3 days to 1 week), we observed a recovery in neuronal activity, with the number of active neurons and their firing rates reaching levels comparable to those observed prior to the microbleed. Notably, this recovery period is longer than what has been observed in superficial microbleeds, where the neural activity typically recovers within one day.[49] These findings suggest that microbleeds in the deep cortex can result in more severe pathologies compared to those in the superficial cortex. From the spatial distribution of active firing neurons over time, the observation of better recovery in the middle layers than in the superficial layers seems counterintuitive. We speculate that there could be due to two potential contributing factors. First, it is possible that different cortical layers consist of distinct subtypes of neurons, and these different types may vary in their vulnerability to the effects of microbleeds. Some subtypes may be more resilient and capable of recovering their activity more efficiently than others. Second, the balance of excitation and inhibition (E/I balance) could also play a role in this phenomenon. For instance, if the deep cortical layers exert more inhibitory input to middle layers, a reduction of overall activity in the deep layers after microbleeds could lead to increased activity in the middle layers. To validate these speculations, future studies could focus on examining different neuronal cell types across different cortical layers to gain a better understanding of their vulnerability and activity change patterns.

Second, we examined the correlations in neuronal activity between neuron pairs within the same layer and across different cortical layers. To our knowledge, this is the first study to examine neuron-neuron activity correlation across the entire cortical column following CMBs. We found that the neuronal activity correlations were significantly lower for both intra-layer and inter-layer neuron pairs from 3 days to 1 week, while the firing rates of these neurons remained unaffected. This alteration in neuron correlations did not fully recover by week 3 or 4, indicating that deep cortical microbleeds can have a lasting impact on the coordinated activity of cortical neuronal networks. This novel finding may provide insights into the higher risk of cognitive decline in individuals with microbleeds, as abnormal neuronal synchronization is closely related to cognitive dysfunctions in various neurological disorders such as schizophrenia, epilepsy, autism, Alzheimer's disease, and Parkinson's disease.[66] Neuronal synchrony is known to be influenced by several factors, including external long-range input, local circuit connectivity, network dynamics, and neuromodulatory systems.[67–69] In addition, the integration of newly generated neurons into existing circuits could potentially impact the overall network activity and synchronization patterns.[70,71] However, the specific mechanisms underlying the observed changes in neural correlation (or connectivity) after microbleeds requires further investigation.

CellPress
OPEN ACCESS

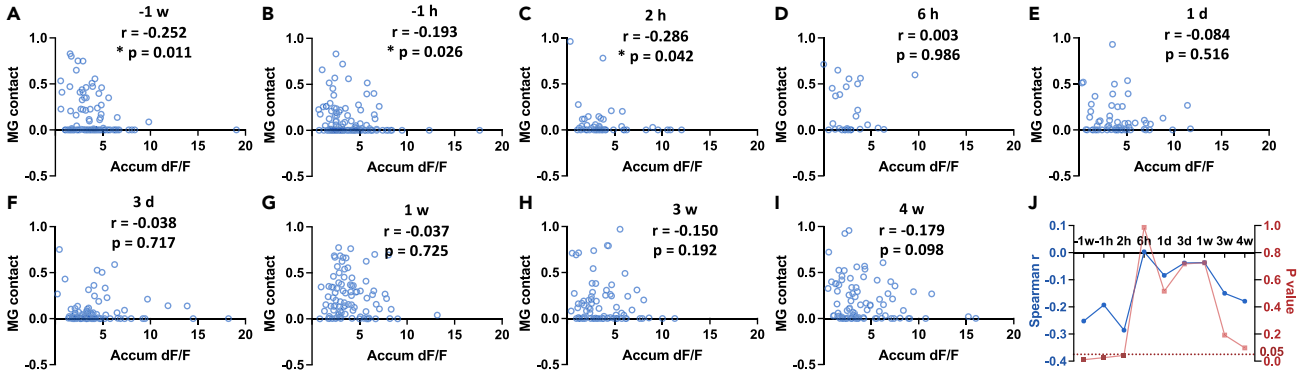

Figure 7. The correlation between microglial contact and neuronal calcium activity change after microbleedings

(A–I) The microglial contact and the accumulative ΔF/F for all detected neurons (29–132 neurons from 3 animals) throughout the cortical column over time. The Spearman correlation r and the p value are provided.

(J) Summary of the Spearman correlation r and p value over time.

Lastly, our results revealed significant changes in microglia-neuron interactions following CMBs. Microglial contact with neuronal soma was significantly elevated at 6 h post-injury and from week 1 to week 4 compared to the pre-injury state. Importantly, this increase in microglial contact was specific to neuron soma and not accompanied by an overall increase in microglial surveillance. Furthermore, we observed dramatic changes in the correlation between microglia-neuron soma contacts and neuronal firing rates from 6 h post-injury. These changes persisted for several days before gradually recovering from week 1 to week 4. These findings highlight chronic alterations in microglial-neuronal interactions following CMBs. During the first a few days after the injury, despite the recovery of neuronal firing rates to pre-injury levels and a similar level of microglial contact as before, the correlation between microglial contact and neural firing rate became non-significant, suggesting a change of functional communication between microglia and neurons during this period. From one-week post-injury, microglial contact increased while neuronal firing rates remained stable, and the correlation gradually recovered over time, suggesting that microglial contact may play a role in the recovery process. The changes observed in microglial contact and neuronal firing rate could be attributed to various factors, including the phenotypic transformation of microglia or alterations in neuronal physiology. Microglia are highly dynamic cells capable of transitioning between different states with distinct effects on neuronal function, depending on the type and time frame of the injury.[72–75] Additionally, it is possible that neurons in the injured cortical region change the sensitivity or threshold to microglial modulation.

In summary, our study demonstrates that unlike the quick recovery observed after superficial CMBs in previous studies, CMBs in the deep cortex can result in long-lasting alterations in the functional activities of both neurons and microglia across cortical depths. These long-lasting network changes may have implications in functional outcomes such as cognitive dysfunctions after microbleeds in various neurovascular diseases such as ICH and cerebral amyloid angiopathy (CAA). Furthermore, this work highlights the importance of vascular health in the context of invasive neural interfacing implants.

Limitations of the study

In recent years, the development of advanced microscopic systems, including multiphoton microscopy, adaptive optics, fiber optics, microendoscope, and microprism implantation, has enabled imaging of deeper brain regions, larger scales, and with faster speeds.[76,77] Among these technologies, microprism implantation stands out as it provides a unique vertical imaging plane that allows for simultaneous imaging of all cortical layers at sub-micron resolution without complicated modifications. It is worth noting that microprism implantation does involve some drawbacks. The implantation process itself causes physical damage to the brain and disrupts the original physiological environment. However, studies have provided evidence that the tissue damage is limited and resolves after several weeks of recovery. Specifically, the receptive field of neurons near the microprism remains unchanged compared to before the implantation,[62] which is also supported by the resolution of inflammatory responses, as indicated by the transition to a "resting state" microglial morphology.[29]

A notable limitation of the present study pertains to the small sample size (n = 3) employed for data analysis. This constraint arose from the inherent challenges associated with chronic microprism implantation and *in vivo* TPM imaging experiments, which are known to have a relatively low success rate. Factors contributing to this limitation encompass instances of unforeseen animal mortalities, infections, and the occurrence of fibrous tissue growth blurring the imaging window. Despite rigorous efforts to mitigate these variables, it is important to acknowledge that the sample size may impact the generalizability of our findings. Therefore, cautious interpretation of the results is advised, particularly in the context of broader population-level implications.

STAR★METHODS

Detailed methods are provided in the online version of this paper and include the following:

- KEY RESOURCES TABLE

SUPPLEMENTAL INFORMATION

Supplemental information can be found online at https://doi.org/10.1016/j.isci.2024.109371.

ACKNOWLEDGMENTS

This work was supported by the National Institute of Neurological Disorders And Stroke of the National Institutes of Health award number R01-NS094404 and under the BRAIN initiative award number R01-NS110564. The content is solely the responsibility of the authors and does not necessarily represent the official views of the National Institutes of Health.

AUTHOR CONTRIBUTIONS

Conceptualization, Q.Y.; Methodology, Q.Y.; Investigation, Q.Y.; Formal analysis, Q.Y.; Writing – Original Draft, Q.Y.; Writing – Review and Editing, Q.Y., A.L.V., and X.T.C.; Funding Acquisition, X.T.C.; Resources, A.L.V. and X.T.C.; Supervision, A.L.V. and X.T.C.

DECLARATION OF INTERESTS

The authors declare no competing interests.

DECLARATION OF GENERATIVE AI AND AI-ASSISTED TECHNOLOGIES IN THE WRITING PROCESS

During the preparation of this work, the authors used ChatGPT3.5 in order to improve language and readability. After using this tool, the authors reviewed and edited the content as needed and take full responsibility for the content of the publication.

Received: September 13, 2023
Revised: December 28, 2023
Accepted: February 26, 2024
Published: March 2, 2024

REFERENCES

1. Ungvari, Z., Tarantini, S., Kirkpatrick, A.C., Csiszar, A., and Prodan, C.I. (2017). Cerebral microhemorrhages: mechanisms, consequences, and prevention. Am. J. Physiol. Heart Circ. Physiol. *312*, H1128–H1143.
2. Li, X., Yuan, J., Yang, L., Qin, W., Yang, S., Li, Y., Fan, H., and Hu, W. (2017). The significant effects of cerebral microbleeds on cognitive dysfunction: an updated meta-analysis. PLoS One *12*, e0185145.
3. Poels, M.M.F., Ikram, M.A., van der Lugt, A., Hofman, A., Niessen, W.J., Krestin, G.P., Breteler, M.M.B., and Vernooij, M.W. (2012). Cerebral microbleeds are associated with worse cognitive function: the Rotterdam Scan Study. Neurology *78*, 326–333.
4. Fisher, M., French, S., Ji, P., and Kim, R.C. (2010). Cerebral microbleeds in the elderly: a pathological analysis. Stroke *41*, 2782–2785.
5. Drouin-Ouellet, J., Sawiak, S.J., Cisbani, G., Lagacé, M., Kuan, W.L., Saint-Pierre, M., Dury, R.J., Alata, W., St-Amour, I., Mason, S.L., et al. (2015). Cerebrovascular and blood–brain barrier impairments in Huntington's disease: potential implications for its pathophysiology. Ann. Neurol. *78*, 160–177.
6. Winkler, E.A., Sengillo, J.D., Sullivan, J.S., Henkel, J.S., Appel, S.H., and Zlokovic, B.V. (2013). Blood–spinal cord barrier breakdown and pericyte reductions in amyotrophic lateral sclerosis. Acta Neuropathol. *125*, 111–120.
7. Hawkins, B.T., and Davis, T.P. (2005). The blood-brain barrier/neurovascular unit in health and disease. Pharmacol. Rev. *57*, 173–185.
8. Cordonnier, C., and van der Flier, W.M. (2011). Brain microbleeds and Alzheimer's disease: innocent observation or key player? Brain *134*, 335–344.
9. Cordonnier, C., Al-Shahi Salman, R., and Wardlaw, J. (2007). Spontaneous brain microbleeds: systematic review, subgroup analyses and standards for study design and reporting. Brain *130*, 1988–2003.
10. Pettersen, J.A., Sathiyamoorthy, G., Gao, F.-Q., Szilagyi, G., Nadkarni, N.K., St George-Hyslop, P., Rogaeva, E., and Black, S.E. (2008). Microbleed topography, leukoaraiosis, and

cognition in probable Alzheimer disease from the Sunnybrook dementia study. Arch. Neurol. *65*, 790–795.
11. Nolta, N.F., Christensen, M.B., Crane, P.D., Skousen, J.L., and Tresco, P.A. (2015). BBB leakage, astrogliosis, and tissue loss correlate with silicon microelectrode array recording performance. Biomaterials *53*, 753–762.
12. Saxena, T., Karumbaiah, L., Gaupp, E.A., Patkar, R., Patil, K., Betancur, M., Stanley, G.B., and Bellamkonda, R.V. (2013). The impact of chronic blood–brain barrier breach on intracortical electrode function. Biomaterials *34*, 4703–4713.
13. Grand, L., Wittner, L., Herwik, S., Göthelid, E., Ruther, P., Oscarsson, S., Neves, H., Dombovári, B., Csercsa, R., Karmos, G., and Ulbert, I. (2010). Short and long term biocompatibility of NeuroProbes silicon probes. J. Neurosci. Methods *189*, 216–229.
14. Sweeney, M.D., Sagare, A.P., and Zlokovic, B.V. (2018). Blood–brain barrier breakdown in Alzheimer disease and other neurodegenerative disorders. Nat. Rev. Neurol. *14*, 133–150.
15. Davalos, D., Ryu, J.K., Merlini, M., Baeten, K.M., Le Moan, N., Petersen, M.A., Deerinck, T.J., Smirnoff, D.S., Bedard, C., Hakozaki, H., et al. (2012). Fibrinogen-induced perivascular microglial clustering is required for the development of axonal damage in neuroinflammation. Nat. Commun. *3*, 1227.
16. Eyo, U.B., and Wu, L.-J. (2013). Bidirectional Microglia-Neuron Communication in the Healthy Brain. Neural Plast. *2013*, 456857.
17. Haynes, S.E., Hollopeter, G., Yang, G., Kurpius, D., Dailey, M.E., Gan, W.-B., and Julius, D. (2006). The P2Y12 receptor regulates microglial activation by extracellular nucleotides. Nat. Neurosci. *9*, 1512–1519.
18. Rogers, J.T., Morganti, J.M., Bachstetter, A.D., Hudson, C.E., Peters, M.M., Grimmig, B.A., Weeber, E.J., Bickford, P.C., and Gemma, C. (2011). CX3CR1 deficiency leads to impairment of hippocampal cognitive function and synaptic plasticity. J. Neurosci. *31*, 16241–16250.
19. Paolicelli, R.C., Bolasco, G., Pagani, F., Maggi, L., Scianni, M., Panzanelli, P., Giustetto, M., Ferreira, T.A., Guiducci, E., Dumas, L., et al. (2011). Synaptic pruning by microglia is necessary for normal brain development. Science *333*, 1456–1458.
20. Schafer, D.P., Lehrman, E.K., Kautzman, A.G., Koyama, R., Mardinly, A.R., Yamasaki, R., Ransohoff, R.M., Greenberg, M.E., Barres, B.A., and Stevens, B. (2012). Microglia sculpt postnatal neural circuits in an activity and complement-dependent manner. Neuron *74*, 691–705.
21. Nimmerjahn, A., Kirchhoff, F., and Helmchen, F. (2005). Resting microglial cells are highly dynamic surveillants of brain parenchyma *in vivo*. Science *308*, 1314–1318.
22. Davalos, D., Grutzendler, J., Yang, G., Kim, J.V., Zuo, Y., Jung, S., Littman, D.R., Dustin, M.L., and Gan, W.-B. (2005). ATP mediates rapid microglial response to local brain injury *in vivo*. Nat. Neurosci. *8*, 752–758.
23. Badimon, A., Strasburger, H.J., Ayata, P., Chen, X., Nair, A., Ikegami, A., Hwang, P., Chan, A.T., Graves, S.M., Uweru, J.O., et al. (2020). Negative feedback control of neuronal activity by microglia. Nature *586*, 417–423.
24. Biber, K., Neumann, H., Inoue, K., and Boddeke, H.W.G.M. (2007). Neuronal 'On'and 'Off'signals control microglia. Trends Neurosci. *30*, 596–602.
25. Ransohoff, R.M., and Cardona, A.E. (2010). The myeloid cells of the central nervous system parenchyma. Nature *468*, 253–262.
26. Li, Y., Du, X.-F., Liu, C.-S., Wen, Z.-L., and Du, J.-L. (2012). Reciprocal regulation between resting microglial dynamics and neuronal activity *in vivo*. Dev. Cell *23*, 1189–1202.
27. Koizumi, S., Shigemoto-Mogami, Y., Nasu-Tada, K., Shinozaki, Y., Ohsawa, K., Tsuda, M., Joshi, B.V., Jacobson, K.A., Kohsaka, S., and Inoue, K. (2007). UDP acting at P2Y6 receptors is a mediator of microglial phagocytosis. Nature *446*, 1091–1095.
28. Kozai, T.D.Y., Vazquez, A.L., Weaver, C.L., Kim, S.-G., and Cui, X.T. (2012). In vivo two-photon microscopy reveals immediate microglial reaction to implantation of microelectrode through extension of processes. J. Neural. Eng. *9*, 066001.
29. Yang, Q., Vazquez, A.L., and Cui, X.T. (2021). Long-term *in vivo* two-photon imaging of the neuroinflammatory response to intracortical implants and micro-vessel disruptions in awake mice. Biomaterials *276*, 121060.
30. Ahn, S.J., Anrather, J., Nishimura, N., and Schaffer, C.B. (2018). Diverse inflammatory response after cerebral microbleeds includes coordinated microglial migration and proliferation. Stroke *49*, 1719–1726.
31. Rotterman, T.M., and Alvarez, F.J. (2020). Microglia dynamics and interactions with motoneurons axotomized after nerve injuries revealed by two-photon imaging. Sci. Rep. *10*, 8648.
32. Yenari, M.A., Kauppinen, T.M., and Swanson, R.A. (2010). Microglial activation in stroke: therapeutic targets. Neurotherapeutics *7*, 378–391.
33. Banati, R.B., Gehrmann, J., Schubert, P., and Kreutzberg, G.W. (1993). Cytotoxicity of microglia. Glia *7*, 111–118.
34. Ju, F., Ran, Y., Zhu, L., Cheng, X., Gao, H., Xi, X., Yang, Z., and Zhang, S. (2018). Increased BBB permeability enhances activation of microglia and exacerbates loss of dendritic spines after transient global cerebral ischemia. Front. Cell. Neurosci. *12*, 236.
35. Fuhrmann, M., Bittner, T., Jung, C.K.E., Burgold, S., Page, R.M., Mitteregger, G., Haass, C., LaFerla, F.M., Kretzschmar, H., and Herms, J. (2010). Microglial Cx3cr1 knockout prevents neuron loss in a mouse model of Alzheimer's disease. Nat. Neurosci. *13*, 411–413.
36. Szalay, G., Martinecz, B., Lénárt, N., Környei, Z., Orsolits, B., Judák, L., Császár, E., Fekete, R., West, B.L., Katona, G., et al. (2016). Microglia protect against brain injury and their selective elimination dysregulates neuronal network activity after stroke. Nat. Commun. *7*, 11499.
37. Neumann, J., Gunzer, M., Gutzeit, H.O., Ullrich, O., Reymann, K.G., and Dinkel, K. (2006). Microglia provide neuroprotection after ischemia. Faseb. J. *20*, 714–716.
38. Ponomarev, E.D., Veremeyko, T., and Weiner, H.L. (2013). MicroRNAs are universal regulators of differentiation, activation, and polarization of microglia and macrophages in normal and diseased CNS. Glia *61*, 91–103.
39. Chen, Z., Jalabi, W., Shpargel, K.B., Farabaugh, K.T., Dutta, R., Yin, X., Kidd, G.J., Bergmann, C.C., Stohlman, S.A., and Trapp, B.D. (2012). Lipopolysaccharide-induced microglial activation and neuroprotection against experimental brain injury is independent of hematogenous TLR4. J. Neurosci. *32*, 11706–11715.
40. Chen, Z., Jalabi, W., Hu, W., Park, H.-J., Gale, J.T., Kidd, G.J., Bernatowicz, R., Gossman, Z.C., Chen, J.T., Dutta, R., and Trapp, B.D. (2014). Microglial displacement of inhibitory synapses provides neuroprotection in the adult brain. Nat. Commun. *5*, 4486.
41. Orihuela, R., McPherson, C.A., and Harry, G.J. (2016). Microglial M1/M2 polarization and metabolic states. Br. J. Pharmacol. *173*, 649–665.
42. Tang, Y., and Le, W. (2016). Differential roles of M1 and M2 microglia in neurodegenerative diseases. Mol. Neurobiol. *53*, 1181–1194.
43. Martinez, F.O., and Gordon, S. (2014). The M1 and M2 paradigm of macrophage activation: time for reassessment. F1000Prime Rep. *6*, 13.
44. Denk, W., Strickler, J.H., and Webb, W.W. (1990). Two-photon laser scanning fluorescence microscopy. Science *248*, 73–76.
45. Stosiek, C., Garaschuk, O., Holthoff, K., and Konnerth, A. (2003). In vivo two-photon calcium imaging of neuronal networks. Proc. Natl. Acad. Sci. USA *100*, 7319–7324.
46. Nishimura, N., Schaffer, C.B., Friedman, B., Tsai, P.S., Lyden, P.D., and Kleinfeld, D. (2006). Targeted insult to subsurface cortical blood vessels using ultrashort laser pulses: three models of stroke. Nat. Methods *3*, 99–108.
47. Tsai, P.S., Blinder, P., Migliori, B.J., Neev, J., Jin, Y., Squier, J.A., and Kleinfeld, D. (2009). Plasma-mediated ablation: an optical tool for submicrometer surgery on neuronal and vascular systems. Curr. Opin. Biotechnol. *20*, 90–99.
48. Allegra Mascaro, A.L., Sacconi, L., and Pavone, F.S. (2010). Multi-photon nanosurgery in live brain. Front. Neuroenergetics *2*, 21.
49. Cianchetti, F.A., Kim, D.H., Dimiduk, S., Nishimura, N., and Schaffer, C.B. (2013). Stimulus-evoked calcium transients in somatosensory cortex are temporarily inhibited by a nearby microhemorrhage. PLoS One *8*, e65663.
50. Rosidi, N.L., Zhou, J., Pattanaik, S., Wang, P., Jin, W., Brophy, M., Olbricht, W.L., Nishimura, N., and Schaffer, C.B. (2011). Cortical microhemorrhages cause local inflammation but do not trigger widespread dendrite degeneration. PLoS One *6*, e26612.
51. Helmchen, F., and Denk, W. (2005). Deep tissue two-photon microscopy. Nat. Methods *2*, 932–940.
52. Hirsch, J.A., and Martinez, L.M. (2006). Laminar processing in the visual cortical column. Curr. Opin. Neurobiol. *16*, 377–384.
53. Markram, H., Toledo-Rodriguez, M., Wang, Y., Gupta, A., Silberberg, G., and Wu, C. (2004). Interneurons of the neocortical inhibitory system. Nat. Rev. Neurosci. *5*, 793–807.
54. Douglas, R.J., and Martin, K.A.C. (2004). Neuronal circuits of the neocortex. Annu. Rev. Neurosci. *27*, 419–451.
55. Lübke, J., and Feldmeyer, D. (2007). Excitatory signal flow and connectivity in a cortical column: focus on barrel cortex. Brain Struct. Funct. *212*, 3–17.
56. Mountcastle, V.B. (1957). Modality and topographic properties of single neurons of cat's somatic sensory cortex. J. Neurophysiol. *20*, 408–434.
57. Mountcastle, V.B. (1997). The columnar organization of the neocortex. Brain *120*, 701–722.

58. Gerfen, C.R., Economo, M.N., and Chandrashekar, J. (2018). Long distance projections of cortical pyramidal neurons. J. Neurosci. Res. *96*, 1467–1475.
59. Ji, X., Ferreira, T., Friedman, B., Liu, R., Liechty, H., Bas, E., Chandrashekar, J., and Kleinfeld, D. (2021). Brain microvasculature has a common topology with local differences in geometry that match metabolic load. Neuron *109*, 1168–1187.e13.
60. Shih, A.Y., Blinder, P., Tsai, P.S., Friedman, B., Stanley, G., Lyden, P.D., and Kleinfeld, D. (2013). The smallest stroke: occlusion of one penetrating vessel leads to infarction and a cognitive deficit. Nat. Neurosci. *16*, 55–63.
61. Chia, T.H., and Levene, M.J. (2009). Microprisms for *in vivo* multilayer cortical imaging. J. Neurophysiol. *102*, 1310–1314.
62. Andermann, M.L., Gilfoy, N.B., Goldey, G.J., Sachdev, R.N.S., Wölfel, M., McCormick, D.A., Reid, R.C., and Levene, M.J. (2013). Chronic cellular imaging of entire cortical columns in awake mice using microprisms. Neuron *80*, 900–913.
63. Dana, H., Mohar, B., Sun, Y., Narayan, S., Gordus, A., Hasseman, J.P., Tsegaye, G., Holt, G.T., Hu, A., Walpita, D., et al. (2016). Sensitive red protein calcium indicators for imaging neural activity. Elife *5*, e12727.
64. Wake, H., Moorhouse, A.J., Jinno, S., Kohsaka, S., and Nabekura, J. (2009). Resting microglia directly monitor the functional state of synapses *in vivo* and determine the fate of ischemic terminals. J. Neurosci. *29*, 3974–3980.
65. Cserép, C., Pósfai, B., Lénárt, N., Fekete, R., László, Z.I., Lele, Z., Orsolits, B., Molnár, G., Heindl, S., Schwarcz, A.D., et al. (2020). Microglia monitor and protect neuronal function through specialized somatic purinergic junctions. Science *367*, 528–537.
66. Uhlhaas, P.J., and Singer, W. (2006). Neural synchrony in brain disorders: relevance for cognitive dysfunctions and pathophysiology. Neuron *52*, 155–168.
67. Bruno, R.M. (2011). Synchrony in sensation. Curr. Opin. Neurobiol. *21*, 701–708.
68. Fu, Y.-X., Djupsund, K., Gao, H., Hayden, B., Shen, K., and Dan, Y. (2002). Temporal specificity in the cortical plasticity of visual space representation. Science *296*, 1999–2003.
69. Gross, J., Schmitz, F., Schnitzler, I., Kessler, K., Shapiro, K., Hommel, B., and Schnitzler, A. (2004). Modulation of long-range neural synchrony reflects temporal limitations of visual attention in humans. Proc. Natl. Acad. Sci. USA *101*, 13050–13055.
70. Carmichael, S.T. (2003). Plasticity of cortical projections after stroke. Neuroscientist *9*, 64–75.
71. Westlake, K.P., and Nagarajan, S.S. (2011). Functional connectivity in relation to motor performance and recovery after stroke. Front. Syst. Neurosci. *5*, 8.
72. Chen, Z., and Trapp, B.D. (2016). Microglia and neuroprotection. J. Neurochem. *136*, 10–17.
73. Biber, K., Owens, T., and Boddeke, E. (2014). What is microglia neurotoxicity (Not)? Glia *62*, 841–854.
74. Benakis, C., Garcia-Bonilla, L., Iadecola, C., and Anrather, J. (2014). The role of microglia and myeloid immune cells in acute cerebral ischemia. Front. Cell. Neurosci. *8*, 461.
75. Gertig, U., and Hanisch, U.-K. (2014). Microglial diversity by responses and responders. Front. Cell. Neurosci. *8*, 101.
76. Yang, Q., and Cui, X.T. (2023). Advanced *in vivo* fluorescence microscopy of neural electronic interface. MRS Bull. *48*, 506–517.
77. Moreaux, L.C., Yatsenko, D., Sacher, W.D., Choi, J., Lee, C., Kubat, N.J., Cotton, R.J., Boyden, E.S., Lin, M.Z., Tian, L., et al. (2020). Integrated Neurophotonics: Toward Dense Volumetric Interrogation of Brain Circuit Activity—at Depth and in Real Time. Neuron *108*, 66–92.

CellPress
OPEN ACCESS

STAR★METHODS

KEY RESOURCES TABLE

REAGENT or RESOURCE	SOURCE	IDENTIFIER
Chemicals, peptides, and recombinant proteins		
Dextran, Cascade Blue™, 3000 MW	Invitrogen	Invitrogen™ D7132
Experimental models: Organisms/strains		
Mouse: B6.129P2(Cg)-Cx3cr1^{tm1Litt}/J	The Jackson Laboratory	RRID:IMSR_JAX:005582
Mouse: Tg(Thy1-jRGECO1a)GP8.31Dkim/J	The Jackson Laboratory	RRID:IMSR_JAX:030526
Software and algorithms		
ImageJ Macros code for "Revealing *in vivo* cellular mechanisms of cerebral microbleeds on neurons and microglia across cortical layers"	Zenodo	https://doi.org/10.5281/zenodo.10602521

RESOURCE AVAILABILITY

Lead contact

Further information and requests for resources and reagents should be directed to and will be fulfilled by the lead contact, X. Tracy Cui (xic11@pitt.edu).

Materials availability

This study did not generate new unique reagents.

Data and code availability

- Data reported in this paper will be shared by the lead contact upon request.
- All original code has been deposited at Zenodo and is publicly available as of the date of publication (https://doi.org/10.5281/zenodo.10602521).
- Any additional information required to reanalyze the data reported in this paper is available from the lead contact upon request.

EXPERIMENTAL MODEL AND STUDY PARTICIPANT DETAILS

CX3CR1-GFP mice (B6.129P2(Cg)-Cx3cr1^{tm1Litt}/J, The Jackson Laboratory, Bar Harbor, Maine) were crossed with Thy1-jRGECO1a mice (Tg(Thy1-jRGECO1a)GP8.31Dkim/J, The Jackson Laboratory, Bar Harbor, Maine) to generate a mouse strain labeling both neural calcium activity and microglial morphology. Three animals (two male, one female) were recruited for this study. All the animals enrolled in the study were at ages between 8 to 20 weeks at which time they underwent the microprism implantation surgery. Influence of sex on the results has not been investigated given the limited sample size in this study. The animals were socially housed until the surgery, residing in a temperature-controlled (21–23°C) and humidity-controlled (40–65%) environment, following a 12-hour light/dark cycle. They had unrestricted access to food and water throughout this period. All experimental protocols were approved by the University of Pittsburgh, Division of Laboratory Animal Resources and Institutional Animal Care and Use Committee in accordance with the standards for humane animal care as set by the Animal Welfare Act and the National Institutes of Health Guide for the Care and Use of Laboratory Animals.

METHOD DETAILS

Microprism implantation surgery

The microprism was assembled and sterilized before the surgery following previously published procedures.[29,62] The 1 mm microprism (#MPCH-1.0, Tower Optical Corporation) was glued to three layers of cover glass (two 3 x 3 mm, one d = 5 mm, Warner Instruments LLC) using optical glue (NOA71, Norland Optical Adhesive). The assembled microprisms were sterilized with ethylene oxide or 70% isopropyl alcohol before the surgery.

Animal anesthesia was induced by an intraperitoneal (IP) injection of ketamine (75 mg/kg) and xylazine (10 mg/kg) cocktail. Anesthetic updates of ketamine (22.5 mg/kg) were applied as needed during the surgery. The mouse's hair was shaved off with an animal clipper and the skin was cleaned with 70% isopropyl alcohol and betadine. Then the animal was head-fixed on a stereotaxic frame (Narishige International USA) and the body temperature was kept at 37°C with a heating pad. A stainless-steel frame (#CF-10, Narishige International USA) was

attached to the skull with dental cement (A-M Systems, Sequim, WA) to hold the animal's head during awake imaging. A 4 x 4 mm cranial window was created over the region of the somatosensory cortex and visual cortex using a dental drill. We performed a durotomy and made a 1 x 1 mm incision perpendicular to the brain surface to slide in the microprism. A silicone sealant (Kwik-sil, World Precision Instruments) was applied onto the brain surface that remain uncovered by the cover glass. UV-curable dental cement (# 062066 Henry Shein) was administered to secure the microprism assembly onto the skull. After surgery, the animal was treated with ketoprofen (5 mg/kg, Zoetis Inc., Kalamazoo, MI) for pain management for three consecutive days.

Two-photon imaging

After recovering from the microprism implantation surgery, the animal was subject to weekly head-fix two-photon imaging on a treadmill. Two-photon fluorescence images were acquired using a two-photon microscopy system (Ultima IV, Bruker Nano, Inc.) with a 16 x 0.8 NA objective lens (Nikon, Inc.). The ultra-fast tunable laser (Insight X3, Newport Spectra-Physics, Inc.) was set to 1025 nm for simultaneous imaging of Thy1-jRGECO1a and CX3CR1-GFP, and 800 nm for imaging the Cascade Blue blood vessel dye (Dextran, 3000 MW, Invitrogen.). Cascade Blue dextran was used as vascular dye and it was injected IP immediately prior to imaging. Time-series imaging was conducted over a field-of-view spanning 815 x 815 μm and matrix size of 512 x 512 pixels at 1 Hz for a total of 20 min. The first 30 s of every acquisition was used for further quantifications. The laser power was kept below 40 mW to prevent potential tissue thermal damage.

Laser ablation of blood vessel

A focal microbleed was generated at around 100 μm from the microprism and at 600~700 μm deep (layer 5/6) following previous publications.[46,60] Briefly, the laser was tuned to 800 nm and scanned over a short line along a micro-sized vessel at 1000 Hz. The power and duration of the laser initiated at 20 mW for 1 s and was increased gradually until the microbleed occurred. A sudden increase in fluorescence intensity and a dark region (red blood cells leakage) around the focused blood vessel were the usual signs of micro bleed generation.

QUANTIFICATION AND STATISTICAL ANALYSIS

All the two-photon imaging data were processed and analyzed using ImageJ or MATLAB. The time-series imaging sequence was first denoised with a median filter and processed with "Correct 3D drift" plugin in ImageJ to correct the micromotion artifact. For the identification of firing neurons, we subtract the mean image of the whole stack from every image and manually labeled the neuron soma using the "oval selection" tool in ImageJ. Using these regions of interest (ROIs) for neuron soma, we recorded the location and the calcium fluorescence activity of each ROI from the raw image sequence (after motion correction).

Cumulative ΔF/F

In MATLAB, we calculated the mean and standard deviation (STD) of the calcium fluorescence intensity for each neuron ROI over the whole 20 min scan. A neural firing threshold was set at mean + STD. Only the calcium fluorescence intensity above that threshold was considered for the calculation of accumulative ΔF/F to indicate the neural firing rate. The ΔF/F ratio was calculated by subtracting the averaged fluorescence intensity from the raw traces and then divided by the mean value. The accumulative ΔF/F was the summation of all the ΔF/F above the threshold during the whole imaging session.

Correlations of neuronal activity

All the neurons in the cortical column of the microbleed (within 150 μm laterally) were included in this analysis. The locations of neurons were categorized into three groups: superficial (> 400 μm), middle (>200 μm and <= 400 μm), and deep (<= 200 μm), based on their depth relative to the micro bleedings. The correlation of neurons was calculated for each pair of neurons using their ΔF/F traces over the 20 min scan.

Microglia intensity distribution

A 300 μm wide subregion around the micro bleed location was selected as the field of interest. The images for microglia fluorescent intensity quantification were averaged from 30 images at a single plane. The Otsu algorithm was used to set a threshold to binarize the image. A microglia ratio was calculated using "plot profile" function in ImageJ, which calculated the ratio of pixels containing microglia fluorescence in each row.

Microglia contact ratio

At every minute, we averaged 30 images of microglial fluorescence in every minute and applied a threshold using the Otsu method. A max intensity projection image was then generated by overlaying 20 binary images over a 20 min scan. From this max projection image, we measured the area covered by microglia over each neuron soma ROI as its microglia contact ratio (Figure 6A).

Microglial surveillance

At every minute, we again averaged 30 images of microglial fluorescence and then applied a standard deviation (STD) projection over the 20 min scan. A higher value in the standard deviation projection indicates where the microglial fluorescence changed more drastically.

The Otsu thresholding method was used to binarize the STD projection image. A 300 μm wide subregion around the micro bleed location was selected for quantification. Then we used "plot profile" function in ImageJ to calculate the ratio of pixels above threshold in each row along the vertical depth.

Statistics

All the statistical analysis was done using the Prism software (GraphPad). Specific statistical tests are described in figure captions. Throughout the text, p-value were presented as *: $p<0.05$, **: $p<0.01$, ***: $p<0.001$, ****: $p<0.0001$.